HHS Public Access

Author manuscript

Clin Cancer Res. Author manuscript; available in PMC 2019 March 15.

Published in final edited form as:

Clin Cancer Res. 2018 March 15; 24(6): 1375–1388. doi:10.1158/1078-0432.CCR-17-2923.

Statins Synergize with Hedgehog Pathway inhibitors for Treatment of Medulloblastoma

Renata E. Gordon[1,5], **Li Zhang**[7], **Suraj Peri**[2], **Yin-Ming Kuo**[3], **Fang Du**[1], **Brian L. Egleston**[2], **Jessica M. Y. Ng**[6], **Andrew J. Andrews**[3], **Igor Astsaturov**[4,5], **Tom Curran**[6], and **Zeng-Jie Yang**[1,7,*]

[1]Cancer Biology Program, Fox Chase Cancer Center, Temple University Health System, Philadelphia, PA, 19111, USA

[2]Biostatistics and Bioinformatics Research Facility, Fox Chase Cancer Center, Temple University Health System, Philadelphia, PA, 19111, USA

[3]Cancer Epigenetics Program, Fox Chase Cancer Center, Temple University Health System, Philadelphia, PA, 19111, USA

[4]Molecular Therapeutics Program, Fox Chase Cancer Center, Temple University Health System, Philadelphia, PA, 19111, USA

[5]Institute of Fundamental Medicine and Biology, Kazan Federal University, Kazan, 420055, Russia

[6]Children's Research Institute, Children's Mercy Kansas City, MO, 64108, USA

[7]Jiangsu Key Laboratory of Neuropsychiatric Diseases and College of Pharmaceutical Sciences, Soochow University, Suzhou, Jiangsu 215123, China

Abstract

Purpose—The role of cholesterol biosynthesis in hedgehog pathway activity and progression of hedgehog pathway medulloblastoma (Hh-MB) were examined *in vivo*. Statins, commonly used cholesterol-lowering agents, were utilized to validate cholesterol biosynthesis as a therapeutic target for Hh-MB.

Experimental Design—Bioinformatic analysis was performed to evaluate the association between cholesterol biosynthesis with hedgehog group MB in human biospecimens. Alterations in hedgehog signaling were evaluated in MB cells after inhibition of cholesterol biosynthesis. The progression of endogenous MB in mice was examined after genetic blockage of cholesterol biosynthesis in tumor cells. Statins alone, or in combination with vismodegib (a FDA-approved Smoothened antagonist), were utilized to inhibit MB growth *in vivo*.

Results—Cholesterol biosynthesis was markedly enhanced in Hh-MB from both humans and mice. Inhibition of cholesterol biosynthesis dramatically decreased Hh pathway activity and

Corresponding author: Dr. Zeng-Jie Yang, Fox Chase Cancer Center, 333 Cottman Avenue, W345, Philadelphia, PA 19111, USA. Phone: +1 215 214 1545; Fax: +1 215 728 2741; zengjie.yang@fccc.edu.

Conflict of interest statement: The authors declare no potential conflicts of interest.

reduced proliferation of MB cells. Statins effectively inhibited MB growth *in vivo*, and functioned synergistically in combination with vismodegib.

Conclusions—Cholesterol biosynthesis is required for Smoothened activity in the hedgehog pathway and it is indispensable for the growth of Hh-MB. Targeting cholesterol biosynthesis represents a promising strategy for treatment of Hh-MB.

Introduction

Cholesterol is a key component of cellular membranes and a precursor for steroid hormones and bile acids. The brain is the most cholesterol-rich organ, containing approximately 20% of total body cholesterol. In the brain, cholesterol is primarily generated by *de novo* synthesis, as the blood-brain barrier in vertebrates prevents its uptake from the bloodstream (1). Almost all cholesterol in the brain is present in an unesterified, free form. Cholesterol is synthesized through a series of ~30 enzymatic reactions, starting with the substrate acetyl-CoA (Fig. 1A). The enzyme 3-hydroxy-3-methylglutaryl-coenzyme A reductase (HMGCR) is rate-limiting for cholesterol biosynthesis. HMGCR converts HMG-CoA to mevalonate and is the target of statins (2). NAD(P) steroid dehydrogenase-like (NSDHL), a 3β-hydroxysterol dehydrogenase, is involved in the removal of two C-4 methyl groups in one of the later steps of cholesterol biosynthesis. Deficiency in NSDHL dramatically impairs cholesterol biosynthesis in both humans and mice (3). In particular, conditional deletion of *Nsdhl* gene in cerebellar granule neuronal precursors, inhibits cholesterol synthesis and dramatically represses proliferation (4). The final step in cholesterol synthesis is catalyzed by the enzyme 24-dehydrocholesterol reductase (DHCR24), which converts desmosterol to cholesterol by saturating the C-24,25 double-bond in the side chain. Triparanol, the first synthetic cholesterol-lowering drug, works by antagonizing DHCR24 (5).

In addition to its function as a component of cell membranes, cholesterol regulates many signaling pathways, including the hedgehog (Hh) pathway. The Hh pathway plays a critical role in brain development and function. In the absence of Hh ligand, the antagonizing receptor Patched1 (Ptch1) suppresses the seven-transmembrane protein, Smoothened (Smo), thus precluding downstream signaling. The interaction between Hh and Ptch1 relieves inhibition of Smo, which then triggers a cascade of events culminating in activation of the glioma-associated oncogenes 1 and 2 (Gli1 and Gli2). Gli proteins translocate into cell nuclei and promote transcription of Hh pathway target genes including *Ptch1* and *Gli1* (6, 7). Extensive evidence suggests that some exogenous oxysterols such as 20 (S)-hydroxycholesterol and 25-hydroxycholesterol, generated by cholesterol oxidation, can activate Smo by binding to a site located in the extracellular cysteine-rich domain (CRD). This indicates that cholesterol derivatives are capable of triggering Hh pathway activation in recipient cells (8–11). Two recent studies revealed that cholesterol itself synergizes with Hh ligand to activate Smo through binding to the CRD (12, 13). The physical interaction between Smo and cholesterol was further confirmed in studies of the crystal structure of Smo (14). These findings suggest that cholesterol functions as a native ligand for Smo activation, and that Hh signaling may be influenced by the local availability of cholesterol.

Insufficient Hh signaling can lead to birth defects, while excessive activity of the Hh pathway is associated with the formation of human malignancies, including medulloblastoma (MB), the most common malignant brain tumor in children. The Hh pathway is activated in approximately 30% of human MB. While the cellular and molecular basis for MB tumorigenesis has been widely studied, the role of cholesterol in MB tumorigenesis has yet to be elucidated.

Previously, several studies claimed that inhibition of cholesterol synthesis promoted apoptosis in MB cells and this effect was greater during co-treatment with the naturally-occurring Hh pathway inhibitor cyclopamine (15–18). However, these effects required the use of statins at levels 1,000-fold greater than the physiological concentrations required to block cholesterol biosynthesis (15–18). In addition, these studies relied on the use of established MB cell lines in which the Hh pathway is now known to be down-regulated (19). An additional confounding problem with these studies, is that they utilized cyclopamine to inhibit the Hh pathway in cultured tumor cells and it has now been demonstrated that, at the concentrations used, cyclopamine causes apoptosis by promoting ceramide production independently of any effects on the Hh pathway (20). Thus, the question remains open as to whether cholesterol pathway inhibitors, alone or in combination with Hh pathway inhibitors, have potential as therapeutic agents in the treatment of Hh-MB.

Here, we demonstrate that there is enhanced cholesterol biosynthesis in Hh pathway-associated MB (Hh-MB) and that cholesterol is required for proliferation of tumor cells *in vitro* as well as tumor growth *in vivo*. Furthermore, we show that cholesterol is necessary for maintaining Smo activity in the absence of Ptch1. Statins, antagonists of cholesterol biosynthesis, exhibited promising therapeutic effects in mouse MB models. Moreover, statins synergized with the clinically approved Smo antagonist, vismodegib, to prevent MB progression *in vivo*. These findings elucidate an important role for endogenous cholesterol in MB tumorigenesis and demonstrate that cholesterol biosynthesis represents a novel therapeutic target for treatment of MB and, potentially, other Hh pathway associated malignancies.

Materials and Methods

Animals

All mice were maintained under barrier conditions in the Laboratory Animal Facility at Fox Chase Cancer Center and all experiments were performed in accordance with procedures approved by the Fox Chase Cancer Center Animal Care and Use Committee. *Nsdhl*$^{fl/fl}$ mice were kindly provided by Dr. Gail Herman (The Ohio State University, Columbus, OH). *Math1-Cre* mice, *Math1-CreER*^{T2} mice, *GFAP-CreER*^{T2} *mice, Ptch1* $^{fl/fl}$ mice, *Ptch1*$^{+/-}$ mice, *R26R-eYFP* mice and *SmoM2 (R26SmoM2)* mice were purchased from the Jackson Laboratory. *CB17/SCID* mice were generated by the animal facility laboratory at Fox Chase Cancer Center.

Tamoxifen (Sigma-Aldrich) was dissolved in corn oil and administrated by oral gavage at a dosage of 200 mg/kg daily during 3 subsequent days. Animals were sacrificed for further analyses after 7 days from initial tamoxifen treatment.

Compounds

The following compounds were used for our *in vitro* and *in vivo* studies: simvastatin (Cayman Chemicals), atorvastatin (Cayman Chemicals), triparanol (Sigma-Aldrich), vismodegib (Chemleader Biochemical) and water-soluble cholesterol (cholesterol-methyl-beta-cyclodextrin, Sigma-Aldrich).

Hh conditioned media (Hh-CM) was prepared by transfection of pcDNA3.1 Shh-N (Addgene) plasmid into 293FT cells. Supernatant collected at 48 hours after transfection was used at 20% for treating NIH 3T3 cells.

Subcutaneous allografts

CB17/SCID male mice of age 6–8 weeks were used for subcutaneous allograft establishment. Cells isolated from tumor-bearing mice in a single-cell suspension in PBS at concentration 2×10^6 cells was mixed with reduced growth factor Matrigel (Corning) in a 20:80 ratio and injected subcutaneously on the flank of *CB17/SCID* mice. 4 weeks following injection, tumor-bearing mice that satisfied initial tumor volume requirement (200–400mm^3) were randomized into experimental groups. Simvastatin DMSO stock was dissolved in mixture of ethanol, 0.1M NaOH and PBS, and administrated in designated dose by intraperitoneal injection. Atorvastatin and vismodegib DMSO stock was dissolved in 0.5% methylcellulose 0.2% Tween-80 and administrated *per os*. Mixture of DMSO, ethanol, 0.1M NaOH and PBS or DMSO and 0.5% methylcellulose 0.2% Tween-80 was used as a vehicle substance. Compounds were administrated in half of the indicated dose twice a day and tumor size measurements were taken every 2 days and tumor volume calculated as described previously (21).

Cell culture

MB cells were suspended in NB-B27 culture medium (Neurobasal, 1 mM sodium pyruvate, 2 mM L-glutamine, B27 supplement, and 1% Pen/Strep, all from Invitrogen) and plated on poly-D-lysine - coated coverslips (Millipore). For BrdU incorporation assay, cells were pulsed with 10 μM BrdU (Millipore) for 2 hours, fixed in 4% PFA and incubated in 4.2mM $MgCl_2$/0.15M NaCl pH5.0 buffer in the presence of 50 U/mL of DNase I (Sigma-Aldrich) at 37°C for 30 minutes.

Primary MEFs were isolated from E13.5 of *Ptch1* $^{fl/fl}$ and *SmoM2* mouse embryos. Dissociated MEFs were cultured in DMEM supplemented with 15% FBS (SH30071.03, HyClone, General Electric), 1mM sodium pyruvate, 2 mM L-glutamine, 1 g/L glucose, penicillin-streptomycin 100 U/ml and 1% non-essential amino acids (all from Life Technologies, unless noted otherwise).

NIH 3T3 and HEK293T cell lines were acquired from ATCC and cultured in DMEM supplemented with 10% FBS, 1% penicillin-streptomycin and 2 mM L-glutamine (all from Life Technologies). All of above cell lines were authenticated and tested for *Mycoplasma* by the Cell Culture Facility at Fox Chase Cancer Center. NIH 3T3 cells and MEFs were starved in serum-free media for 24 hours before virus infection or Hh treatment. All *in vitro* studies were performed in serum-free environment.

For synergistic effects experiments, NIH 3T3 cells were starved for 24 hours before treatment with 20% Hh-CM. Hh-treated NIH 3T3 cells and freshly isolated *Ptch1*$^{+/-}$ MB cells were then incubated with 0.001 to 1μM WSC for 18–20 hours to saturate Smo, and 1 nM vismodegib for additional 48 hours.

Lentiviral production

Lentiviral production was performed by utilizing *Nsdhl* shRNAs and scrambled shRNA (Genocopiea, MSH029806), pLUT Gli1-HA, pMD2.G and psPAX2 (Addgene) plasmids in accordance to the standard protocol.

Histology and immunohistochemistry

For histological analyses, cerebella were removed from mice and fixed in 10% neutral-buffered formalin overnight. Samples were embedded in paraffin, 5 μm sagittal sections were prepared and stained for ABCA1 (Abcam, ab18180, 1:500), NSDHL (Proteintech, 15111-1-AP, 1:100) and SREBP2 (Abcam, ab30682, 1:100).

Frozen sections were prepared according to standard protocol (22). Briefly, tissue was fixed in 4% PFA overnight, cryoprotected in 30% sucrose overnight and frozen in O.C.T. (Fisher Scientific). 12 μm sagittal sections were prepared with a cryostat (Leica). Cultured MB cells were fixed in 4% PFA for 15 minutes.

Tissue sections or cultured cells were permeabilized, blocked with 10% normal goat serum in PBS, 0.1% Triton-X100 and incubated overnight in primary antibody mix against Ki67 (Abcam, ab15580, 1:1000), NeuN (Abcam, ab104224, 1:200), Cleaved Caspase 3 (Cell Signaling, CST9661, 1:500), BrdU (Sigma-Aldrich, B8434, 1:500), mCherry (Abcam, ab167453, 1:500), Zic1 (Generous gift from Dr. Rosalind Segal at Dana Farber Research Institute, 1:200), S100β (Sigma-Aldrich, S2532, 1:500), GFP (Life Technologies, A11122, 1:500), GFAP (BD, 556330,, 1:500). After 2 hours of incubation in secondary antibodies, samples were counterstained with DAPI and mounted with Fluoromount-G. For fillipin staining experiments, MB sections were incubated with 2 mg/ml filipin (Sigma-Aldrich) for 2 hours, counterstained with DRAQ5 and mounted with Fluoromount-G.

Western blotting

Cells and tissues were lysed in RIPA buffer (Thermo) supplemented with protease (Roche) and phosphatase (Thermo) inhibitors cocktail. Total protein lysates were separated in 8% SDS-PAGE and transferred on PVDF membrane. Membranes were probed with antibodies against Gli1 (Cell Signaling, CST2534, 1:1000), NSDHL (Proteintech, 15111-1-AP, 1:1000), Ptch1 (Novus Biologicals, MAB41051, 1:1000), GAPDH (Sigma-Aldrich, G8795, 1:1000). Western Blot signals were detected with SuperSignal West Pico Substrate and exposed on films.

qPCR

RNA was isolated using TRI reagent (Sigma-Aldrich) in RNase-free conditions. cDNA was synthesized using oligo(dT) and Superscript II reverse transcriptase (Invitrogen). Quantitative PCR reactions were performed in triplicates using iQ SYBR Green Supermix

(Bio-Rad) and the Bio-Rad iQ5 Multicolor Real-Time PCR Detection System. Primer sequences are available upon request.

Mass-spectrometry and fluorometric cholesterol assay

Cells or tissue samples were washed with ice-cold DPBS, and lipids were extracted using a Bligh/Dyer procedure, in which 6 mL of 1:2 (v/v) chloroform:methanol was added to the sample. $^{2}H_{6}$-26,26,26,27,27,27-cholesterol (Sigma-Aldrich) was used as the internal standard spiked in individual samples. The cholesterol-containing chloroform layer was collected and evaporated under a gentle, dried nitrogen stream at 35°C. The dried samples were re-dissolved in 200μl methanol and analyzed by ultra-performance liquid chromatography-tandem mass spectrometry (UPLC-MS/MS). The peaks of samples were processed and analyzed using Xcalibur, version 2.1.

Statistical analysis

All studies were performed at least in three independent replicates with outcomes reflected on photographs, graphs or film scans. Material collection time points were designed in accordance to previously published literature. During data analysis, no exclusion criteria were applied. Two-sided Student's *t* tests were performed to determine the statistical significance of the difference in means between samples in the experiments reported. $P<0.05$ was considered statistically significant. Error bars represent the SEM. Data handling and statistical processing was performed using Microsoft Excel.

The raw gene expression data used for analyzing subtype specific pathway alterations in MB, were obtained from GEO (GSE21140) and normalized using RMA. Gene Set Variation Analysis (GSVA) (23) on the RMA normalized expression data was applied to identify pathways that are enriched in a single sample (method arguments: function='gsva'; mx.diff='FALSE'; verbose=FALSE). Over 4900 gene sets compiled from all gene sets available in MsigDB including KEGG and Biocarta pathways were used for enrichment analysis. In order to identify pathways that differ significantly among subtypes, Kruskal–Wallis test was used to analyze the enrichment scores resulting from GSVA.

To compare the progression rates (Fig. 5A, 6A and 6C), we used generalized linear regression models assuming Gamma family and log links. We used the following growth curve model to test for synergy:

$$\log(\mathrm{E}[\mathrm{Y}|\mathrm{V},\mathrm{S},\mathrm{D}])=\beta_0+\beta_1\mathrm{V}+\beta_2\mathrm{S}+\beta_4\mathrm{V}\times\mathrm{S}+(\beta_3+\beta_5\mathrm{V}+\beta_6\mathrm{S}+\beta_7\mathrm{V}\times\mathrm{S})\times\mathrm{D},$$

where Y=tumor volume, D=day, V=vismodegib, S=statin, and E[Y|V,S,D]=conditional expectation (i.e. average). β_5 and β_6 test for additive drug growth effects, and the interaction term, β_7, tests for synergistic/antagonistic drug growth effects. Synergism was concluded if the direction of β_7 enhanced drug effects and $p<0.05$ (24).

Results

Hh-MB exhibit dysregulated cholesterol metabolism

Human MB comprises at least four subgroups including Hh, Wnt, Group 3 and Group 4 based on distinct gene expression profiles (25, 26). Hh-MB arises from aberrant activation of the Hh pathway in the developing cerebellum. To examine pathway alterations among MB subgroups, we analyzed transcriptomes of 103 primary human MB by Geneset Variation Analysis (GSVA) (23). This analysis uncovered 363 gene sets and pathways (GSPs) that exhibit selective enrichment across the four subtypes. The significant GSPs ranking high in the list included the Hh and Netrin pathways known to play roles in Hh-MB tumorigenesis (Table S1 and Fig. 1B–1D) (27), In addition, we observed that cholesterol and sterol biosynthesis GSPs were associated with Hh-MB but not the other 3 MB subgroups. The enrichment scores of both steroid and cholesterol biosynthesis pathways were higher in Hh-MB than the other 3 subtypes (Fig. 1C). Most of the genes in these two pathways are identical and their expression levels are remarkably elevated in Hh-MB (Fig. 1D). These data suggest an unexpected association between cholesterol biosynthesis and Hh-MB.

Mice heterozygous for *Ptch1* (hereafter referred as $Ptch1^{+/-}$ mice) are widely used in preclinical studies for Hh-MB as 15–20% of mice spontaneously develop MB in cerebella after 3–4 months of age (28) and this is accelerated to 100% in the absence of p53 (29). Constitutive activation of the Hh pathway as a consequence of loss of *Ptch1* heterozygosity is critical for MB formation in $Ptch1^{+/-}$ mice. To investigate the possible association between cholesterol biosynthesis and tumorigenesis in Hh-MB, we examined the expression of proteins involved in cholesterol homeostasis in MB tissue from $Ptch1^{+/-}$ mice by immunohistochemistry. Cholesterol homeostasis is tightly regulated by a complex protein network responsible for its import, synthesis and export (30). As shown in Fig. 1E, expression of NSDHL was significantly up-regulated in MB tissue compared with adjacent normal cerebellar tissue, suggesting there is increased cholesterol synthesis in tumor tissue. Transcription of ATP-binding cassette transporter 1 (ABCA1), an established regulator of cellular cholesterol homeostasis, is normally driven by increased accumulation of intracellular cholesterol (31) and sterol regulator element-binding protein 2 (SREBP2) is well known to upregulate genes involved in cholesterol biosynthesis and uptake (32). The levels of both ABCA1 and SREBP2 were substantially elevated in tumors, compared with adjacent normal cerebellum (Fig. 1F–1G). These data imply that there is enhanced synthesis of cholesterol in Hh-MB.

MB growth relies on de novo cholesterol biosynthesis

Having observed upregulation of cholesterol biosynthesis genes in Hh-MB, we investigated the possible function of cholesterol in MB tumorigenesis. MB cells isolated from $Ptch1^{+/-}$ mice were infected with a lentivirus carrying mCherry-tagged *Nsdhl* shRNAs or scrambled shRNA. At 48 hours following viral infection, NSDHL protein expression was effectively repressed by *Nsdhl* shRNAs (Fig. 2A). Expression of Gli1 was significantly reduced in NSDHL-deficient MB compared with scrambled shRNA-infected MB cells (Fig. 2A), indicating that *Nsdhl* knockdown impaired Hh pathway activity. We next examined proliferation of MB cells at 48 hours following viral infection. As shown in Fig. 2B–2D,

approximately 15% of scrambled shRNA-infected MB cells were positive for BrdU, compared with only 4–6% BrdU positive cells among NSDHL-deficient MB cells. These data suggest that cholesterol synthesis is critical for proliferation and Hh pathway activity in MB cells.

We next examined proliferation of MB cells *in vivo* after genetic ablation of cholesterol biosynthesis in tumor cells. Hh-MB cells specifically express the helix-loop-helix transcription factor Math1 (22). To establish an appropriate assay system, *Math1-CreER^{T2}* mice, capable of expressing a tamoxifen-inducible Cre recombinase only in Math1-expressing cells, were crossed with *Ptch1$^{+/-}$* mice and *R26R-eYFP* mice carrying a loxP-flanked STOP cassette upstream of the *eYFP* gene (33). After tumors were established, *Math1-CreER^{T2}/R26R-eYFP/Ptch1$^{+/-}$* mice were treated with tamoxifen by oral gavage. As shown in Fig. 2E, most of the tumor cells positive for Zic1 (34) also expressed YFP, but no astrocytes (S100β positive) were positive for YFP (Fig. 2F). These data indicate that *Math1-CreER^{T2}* mice can be utilized to target MB cells *in vivo*.

To disrupt cholesterol biosynthesis in MB cells, we utilized conditional *Nsdhl$^{fl/fl}$* knockout mice, in which a portion of the *Nsdhl* gene is flanked by loxP sites (4), crossed with *Math1-CreER^{T2}* mice and *Ptch1$^{+/-}$* mice. *Math1-CreER^{T2}/Nsdhl$^{fl/fl}$/Ptch1$^{+/-}$* mice and *Nsdhl$^{fl/fl}$/Ptch1$^{+/-}$* mice were orally treated with tamoxifen after tumors were fully established. At 7 days after tamoxifen treatment, MB tissues from *Math1-CreER^{T2}/Nsdhl$^{fl/fl}$/Ptch1$^{+/-}$* mice and *Nsdhl$^{fl/fl}$/Ptch1$^{+/-}$* littermates were examined for expression levels of NSDHL and Gli1 as well as the amount of intracellular cholesterol present in the tumor. As shown in Fig. 2G, after tamoxifen treatment NSDHL was depleted in MB tissues obtained from *Math1-CreER^{T2}/Nsdhl$^{fl/fl}$/Ptch1$^{+/-}$* mice. Moreover, Gli1 expression was decreased in MB tissue from *Math1-CreER^{T2}/Nsdhl$^{fl/fl}$/Ptch1$^{+/-}$* mice compared with tumor tissue from *Nsdhl$^{fl/fl}$/Ptch1$^{+/-}$* mice, suggesting that Hh signaling was compromised in *Nsdhl*-deficient MB. In addition, the amount of cholesterol in tumor tissue was reduced by 50±10% after tamoxifen treatment, as revealed by mass-spectrometry analysis (Fig. 2H), indicating that *Nsdhl* deletion effectively suppressed cholesterol biosynthesis in tumor cells. We next examined the proliferation and survival of cholesterol-deficient MB cells *in vivo*. As shown in Fig. 2I—2I″, cell proliferation was reduced by 50±5% in *Nsdhl*-deficient MB tissue compared control MB tissue from *Nsdhl$^{fl/fl}$/Ptch1$^{+/-}$* mice, as shown by immunostaining for Ki67. MB cells that remained proliferating were predominately located in regions of tumor tissue in which cholesterol was not completely depleted based on filipin staining (Fig. S1). It appeared that most of the *Nsdhl*-deficient tumor cells differentiated based on the expression of neuronal differentiation marker NeuN (Fig. 2J—2J″). Increased apoptosis was also detected by cleaved caspase 3 (CC3) immunostaining of tumor tissue after *Nsdhl* deletion compared with that in control tumor tissue (Fig. 2K—2K″). Consistent with our findings in NSDHL-deficient MB tissues, expression of Hh pathway target genes, including *Gli1*, *Myc-N* and *Ptch1,* was significantly repressed after *Nsdhl* deletion (Fig. 2L). The above data demonstrate that *de novo* biosynthesis of cholesterol in MB cells is required for proliferation and tumor growth.

Astrocytes expressing glial fibrillary acidic protein (GFAP) were abundantly present and intermingled with tumor cells in MB tissue (Zic1 positive, Fig. S2A). To test whether

cholesterol from astrocytes is required for MB progression, we examined MB cell proliferation after disrupting cholesterol synthesis in astrocytes by using *GFAP-CreER*^{T2} mice (35). For this purpose, we generated *GFAP-CreER*^{T2}*/Nsdhl*$^{fl/fl}$*/Ptch1*$^{+/-}$ mice, and *Nsdhl*$^{fl/fl}$*/Ptch1*$^{+/-}$ mice as a control. These mice were treated with tamoxifen by oral gavage after tumors were established at approximately 30 weeks of age. As shown in Fig. S2B–2D″, no obvious alterations in the proliferation, differentiation or apoptosis were found in MB tissue after *Nsdhl* deletion in astrocytes in *GFAP-CreER*^{T2}*/Nsdhl*$^{fl/fl}$*/Ptch1*$^{+/-}$ mice, compared with that in *Nsdhl*$^{fl/fl}$*/Ptch1*$^{+/-}$ mice. These data suggest that astrocyte-derived cholesterol is dispensable for MB growth.

Cholesterol is required for Smo activation

To investigate the role of cholesterol in Hh pathway activation, we treated MB cells from *Ptch1*$^{+/-}$ mice with simvastatin in short-term cultures. Under these conditions the Hh pathway remains active whereas it is repressed in long-term cultures (19). Approximately 48 hours after treatment, cells were harvested to determine the level of Gli1 expression by western analysis. As shown in Fig. 3A, the expression levels of Gli1 declined in MB cells as the concentration of simvastatin was increased. To confirm that compromised Hh pathway activity in MB cells after treatment with simvastatin is a consequence of reduced cholesterol levels, we added water-soluble cholesterol (WSC) to the tumor cell cultures. As shown in Fig. 3A, the addition of exogenous cholesterol rescued Gli1 expression in simvastatin-treated MB cells. These data suggest that simvastatin inhibits Hh pathway activity in MB cells by disrupting cholesterol biosynthesis.

To identify which component of the Hh pathway is regulated by cholesterol, we investigated the effect of cholesterol on Hh ligand signaling in NIH 3T3 cells. As expected, Hh treatment significantly up-regulated Gli1 expression in NIH 3T3 cells. The induction of Gli1 by Hh ligand was blocked by simvastatin or triparanol and this was overcome by addition of exogenous WSC to the culture medium (Fig. 3B). These data confirm that cholesterol is necessary for transduction of Hh pathway activity from ligand to target gene expression.

We next generated primary mouse embryonic fibroblasts (MEFs) from *Ptch1*$^{fl/fl}$ mice carrying exons 1 and 2 of the *Ptch1* gene flanked by loxP sites, and from *SmoM2* mice carrying loxP-flanked STOP cassette placed upstream of constitutively active Smo (36). MEFs were then infected with a lentivirus carrying Cre recombinase to delete Ptch1 or activate Smo, or with a control lentivirus carrying an empty vector. At 48 hours after infection with a Cre-bearing virus, Hh pathway activity was elevated in both models, as determined by increased levels of Gli1 expression (Fig. 3C–3D). Importantly, treatment with simvastatin or triparanol dramatically inhibited Gli1 expression in *Ptch1*-deficient MEFs and this inhibition was overcome by addition of exogenous cholesterol, indicating that cholesterol is required for Hh pathway activation resulting from *Ptch1* deletion. In contrast, treatment of cells harboring an activated Smo gene with simvastatin or triparanol treatment failed to reduce Gli1 expression, indicating that cholesterol is dispensable for Hh pathway signaling resulting from constitutively active Smo. Consistent with the results described above, we found that increased levels of Ptch1 caused by overexpression of Gli1 were not altered by treatment with simvastatin or triparanol (Fig. 3E). Taken together, our data

demonstrate that cholesterol is required for Smo function in the Hh signaling pathway (Fig. 3F).

Antagonists of cholesterol synthesis inhibit MB cell proliferation

Since cholesterol is necessary for Hh signaling, we hypothesized that inhibition of cholesterol synthesis might suppress MB cell proliferation. To test this idea, we examined MB cell proliferation in the presence or absence of simvastatin or triparanol. MB cells isolated from *Ptch1*$^{+/-}$ mice were briefly cultured in the presence of cholesterol inhibitors or vehicle for 48 hours, and examined for proliferation by immunocytochemistry. As shown in Fig. 4A, about 60% of MB cells were proliferating (Ki67 positive) in control cultures, but the percentage of proliferating cells declined significantly in a dose-dependent manner as the concentration of simvastatin was increased (Fig. 4B–4D). Reduced proliferation of MB cells was also observed after treatment with triparanol (Fig. 4E). As shown in Fig. 4G–4J, addition of exogenous cholesterol rescued the proliferation repressed by simvastatin or triparanol treatment (Fig. 4K), suggesting that reduced proliferation of MB cells treated with simvastatin or triparanol was indeed due to cholesterol deficiency. We also noted that proliferation of vehicle treated cells increased upon exposure to exogenous cholesterol indicating that the endogenous levels are rate-limiting under the experimental conditions used (Fig. 4F). These data indicate that antagonists of cholesterol biosynthesis significantly inhibit MB cell proliferation. We next tested whether pharmaceutical inhibition of cholesterol synthesis could be utilized to treat MB. For this purpose, we generated a MB model by subcutaneous injection of CB17/SCID mice with MB cells isolated from *Ptch1*$^{+/-}$ mice, as previously described (19). This model was validated during the development of vismodegib and shown to accurately predict clinical responses in humans (37, 38). In contrast, human tumor cell lines fail to sustain Hh pathway activity; therefore, they cannot be used to test the efficacy of inhibitors of Hh pathway activity (19). After the allograft tumor volume reached 200–400 mm^3, mice were treated by intraperitoneal injection of 20 mg/kg/day simvastatin, 40 mg/kg/day simvastatin, or vehicle. No significant difference in tumor growth was observed between the control and 20 mg/kg/day simvastatin treatment ($p=0.32$) (Fig. 5A). The volume of tumors from the group of mice treated with 20 mg/kg/day simvastatin was comparable with that from the control group after 21 days of treatment (Fig. 5B). However, tumor volume was dramatically reduced after treatment with 40 mg/kg/day simvastatin, compared with either vehicle ($p<0.001$) or with 20 mg/kg/day ($p<0.001$), suggesting that simvastatin at a dose of 40 mg/kg/day effectively suppressed MB growth *in vivo*. To determine the mechanism responsible for suppressed tumor growth by simvastatin, we examined the proliferation and survival of tumor cells following simvastatin treatment by immunohistochemistry. Proliferation of MB cells (Ki67 positive) was markedly reduced after simvastatin treatment (Fig. 5C—5C″) compared with vehicle. Moreover, simvastatin treatment promoted significant differentiation, evidenced by up-regulation of NeuN in MB tissue (Fig. 5D—5D″). In addition, an increased number of apoptotic cells (CC3 positive) were observed in tumor tissues after simvastatin treatment, indicating increased apoptosis (Fig. 5E—5E″). Based on qPCR and western analyses, Gli1 mRNA and protein expression were significantly down-regulated in tumors treated with 40 mg/kg/day simvastatin compared with the vehicle control (Fig. 5F–5H), suggesting simvastatin compromised Hh signal transduction in MB cells. In addition, *Ptch1*$^{+/-}$ mice with established MB were treated

with 40mg/kg/day simvastatin for 2 weeks. As shown in Fig. S3A–D, simvastatin markedly inhibited tumor cell proliferation and promoted tumor cell differentiation in MB tissue. Moreover, activation of Hh pathway in MB tissue was repressed following simvastatin treatment. Together, these data demonstrate that simvastatin treatment can reduce MB growth *in vivo*.

The SmoM2 mutation results in an amino acid substitution (W535L) in the seventh transmembrane domain, creating a constitutively active form of Smo by disrupting G-protein coupling (39). The SmoM2 mutation has been observed in human MB and in basal cell carcinoma (39, 40). Hh signaling in MEF cells carrying a SmoM2 mutation was not affected by simvastatin treatment (Fig. 3D), suggesting that activation of Hh pathway by SmoM2 is not dependent on cholesterol. To test the effect of simvastatin on the growth of MB resulting from *Smo* activation, we generated MB using *Math1-Cre/SmoM2* mice as previously described (41). As shown in Fig. S4A–C, proliferation of MB cells *in vitro* was not altered after simvastatin treatment. In the MB allograft mouse model generated using MB cells from *Math1-Cre/SmoM2* mice, no obvious inhibition of MB growth was observed after simvastatin treatment (Fig. S4D–E). These data indicate that MB cells carrying the SmoM2 mutation are resistant to simvastatin treatment and that the SmoM2 mutation uncouples Smo from cholesterol dependency.

Statins synergize with Smo antagonist in MB treatment

Previous studies reported that oxysterols and cholesterol bind to Smo at CRD binding site, which is distinct from the binding pocket of the conventional Smo antagonist, vismodegib (42). This led us to investigate the possible synergistic effects of statins and vismodegib in the treatment of MB. For this purpose, mice bearing subcutaneous allograft tumors from *Ptch1*$^{+/-}$ mice were treated with vismodegib, simvastatin or the two in combination. Consistent with previous reports (43), treatment with vismodegib at 5 mg/kg/day reduced Hh-MB growth (Fig. 6A–B). However, combined treatment with vismodegib and simvastatin resulted in a complete inhibition of Hh-MB progression. Although 20 mg/kg/day simvastatin exhibited no inhibitory effect on MB growth ($p=0.32$), 5 mg/kg/day vismodegib in combination with 20 mg/kg/day simvastatin resulted in an additional reduction in tumor growth compared with vismodegib alone ($p<0.001$). These data suggest that simvastatin and vismodegib act synergistically to prohibit tumor growth. The synergistic effect of simvastatin and vismodegib in MB treatment was confirmed statistically as explained in the Materials and Methods section.

CB17/SCID mice carrying allografts of *Ptch1*$^{+/-}$ MB were also treated with another HMG-CoA inhibitor, atorvastatin, alone or combined with vismodegib. Atorvastatin treatment at 10mg/kg/day ($p<0.001$) or 40mg/kg/day ($p<0.001$) significantly repressed tumor growth compared with vehicle treatment, confirming inhibitory effects of statins on MB growth (Fig. 6C–D). Moreover, 10 mg/kg/day atorvastatin dramatically enhanced the inhibitory effects of vismodegib on MB growth, when compared with vismodegib treatment alone ($p<0.001$), further confirming the synergistic effects of statins and vismodegib in inhibiting MB growth.

Having observed the synergistic effects of statins and vismodegib in MB treatment, we next investigated whether cholesterol could affect the interaction between Smo and vismodegib. For this purpose, we pretreated NIH 3T3 cells and *Ptch1*$^{+/-}$ MB cells with WSC, and then examined the inhibitory effects of vismodegib on Hh signaling based on Gli1 protein expression. As expected, vismodegib significantly inhibited Gli1 expression in Hh-treated 3T3 cells (Fig. 6E) and *Ptch1*$^{+/-}$ MB cells (Fig. 6F). However, pretreatment with cholesterol abrogated vismodegib-induced inhibition of Hh signaling in a dose-dependent manner. These data suggest that, at high concentrations, binding of cholesterol to Smo may prevent its interaction with vismodegib, perhaps through an allosteric effect, providing a potential basis for the synergistic effect of statins and vismodegib in MB treatment.

Discussion

Cholesterol is an essential component of plasma membranes and it plays an important role in cell membrane organization, dynamics and function. During normal development, cholesterol homeostasis is tightly regulated by a complex protein network involving importation, biosynthesis, exportation, metabolism and esterification. Altered expression levels, and mutations of genes involved in the cholesterol homeostasis pathways, have been identified in many human malignancies, including glioblastoma, pancreatic cancer and melanoma (44). Impaired cholesterol homeostasis in tumor cells influences tumor progression and dictates the sensitivity of tumor cells to chemotherapy (45), although it is still debated whether cellular cholesterol levels influence tumor initiation. Our studies reveal enhanced expression of genes associated with cholesterol biosynthesis in Hh-MB, suggesting that the intracellular cholesterol levels in tumor cells are elevated. Inactivating mutations of *Ptch1*, the most common mutation in Hh-MB, may also contribute to increased cholesterol levels in tumor cells, in that Ptch1 is involved in cholesterol efflux from cells (46).

Extensive evidence indicates that some exogenous oxysterols such as 20 (S)-hydroxycholesterol and 25-hydroxycholesterol generated by cholesterol oxidation, activate Smo by binding to a site located in the extracellular CRD, demonstrating that cholesterol derivatives are capable of triggering Hh pathway activity (8–11). However, it is unclear whether these oxysterols are physiological activators of Smo, given that the endogenous levels are significantly lower than the EC_{50} for Hh pathway activation. In this study, we found that, upon inhibition of cholesterol biosynthesis, using proximal and distal inhibitors (simvastatin and triparanol, respectively), Hh pathway activity in MB cells and fibroblasts was significantly repressed. Proliferation of MB cells and tumor growth *in vivo* was repressed after pharmacological or genetic inhibition of cholesterol biosynthesis. These data suggest that endogenous cholesterol biosynthesis is important for Hh pathway activity. Compromised Hh pathway activity was observed in cholesterol-deficient fibroblasts after loss of Ptch1 but not following constitutive activation of Smo or after overexpression of Gli1. These data indicate that cholesterol biosynthesis is required for Smo to function in Hh signaling. Recent findings that cholesterol synergizes with Hh to activate Smo through binding to the extracellular CRD (12, 13), are consistent with the conclusion that cholesterol, but not oxysterols, functions as the endogenous ligand responsible for Smo activation during Hh pathway signaling, and that Ptch1 inhibits Smo by counteracting its

activation by cholesterol. Thus, cholesterol plays a unique role as a second messenger in vertebrate Hh signaling, by mediating the functional interaction between Ptch1 and Smo. These findings resolve a long-lasting question of how Ptch1 suppresses Smo activity and they identify cholesterol as a critical component for Smo activation by Ptch1-mediated Hh signaling. Simvastatin also inhibits proliferation of Group 3 MB, which are associated with activating mutations in *c-Myc* and dysfunctional *p53* (47). These findings imply that cholesterol may regulate many other signaling pathways in MB in addition to Hh signaling.

The blood-brain barrier efficiently blocks transport of cholesterol from the bloodstream into the brain. Therefore, nearly all brain cholesterol is produced via *de novo* synthesis (1). Recently it has been demonstrated that tumor cells in glioblastoma multiforme, the most malignant brain tumor in adults, exclusively acquire cholesterol from astrocytes (45). In our studies, conditional inhibition of cholesterol biosynthesis in tumor cells dramatically inhibited MB cell proliferation and promoted the differentiation of tumor cells, whereas, disruption of cholesterol synthesis in astrocytes had no effects in MB cell proliferation and survival. These observations suggest that MB cells predominately rely on *de novo* synthesis of cholesterol. In our studies, cholesterol was not completely depleted after deletion of the *Nsdhl* gene in MB cells in *Math1-CreER*^{T2}*/Nsdhl*$^{fl/fl}$*/Ptch1*$^{+/-}$ mice following tamoxifen treatment. Based on filipin staining, some regions of the tumor tissue were enriched with cholesterol. Such incomplete depletion of cholesterol in tumor tissue could be due to insufficient Cre recombination and/or inadequate tamoxifen penetration. However, we cannot completely exclude the possibility that tumor cells at least partially acquire cholesterol from their microenvironment. Nevertheless, proliferating MB cells predominantly accumulated in cholesterol-enriched tumor regions of *Math1-CreER*^{T2}*/ Nsdhl*$^{fl/fl}$*/Ptch1*$^{+/-}$ mice, further confirming that cholesterol is critical for MB growth.

The observation of Hh pathway dysregulation in tumors has caused it to be an attractive pharmacological target for cancer treatment for many years. All the available Hh pathway inhibitors being studied in clinical trials target Smo. Our studies demonstrate that cholesterol biosynthesis is essential for MB progression. Statins effectively inhibited MB cell proliferation and suppressed tumor growth. The excellent safety profile, together with low cost and ready availability of statins, make cholesterol biosynthesis a promising target for MB treatment and perhaps other malignancies involving Hh signaling.

Smo inhibitors cause developmental bone abnormalities in young mice (43). Therefore, they are not recommended for use in young children. Potentially, the combined use of vismodegib and statins could permit the use of lower doses of Smo inhibitors, potentially reducing the extent of bone toxicity in the pediatric Hh-MB patient population. Currently, statins are being used to manage dyslipidemia in some children and are among the drugs approved for use in children (48, 49). So far there have been no reports of bone toxicities or other phenotypes that could be ascribed to Hh pathway inhibition. Nevertheless, further studies are warranted to test the potential for combined toxicities of Smo inhibitors and statins in developing animal models prior to their use in children.

The potential efficacy of statins in Hh-MB therapy depends on which underlying mutation the tumor harbors in the Hh pathway. Among Hh-MB patients, approximately 80% of adult

together with 50% of infant and childhood patients harbor mutations in Hh, Ptch1 or Smo, who are most likely to respond to Smo antagonists including statins (40). However, MB carrying the SmoM2 mutation are predicted to be resistant to Smo inhibitors as well as cholesterol inhibitors. Similarly, around 45% of infant and childhood Hh-MB patients frequently harbor mutations downstream of Smo, such as Sufu or Gli2 (40), rendering these tumors intrinsically resistant to any drugs targeting Smo.

Our studies reveal the synergistic effects of statin and vismodegib in treating MB. It has been confirmed that cholesterol activates Smo through interaction with the CRD region, which is distinct from the binding site of vismodegib. Recent structural studies found that binding with vismodegib precludes the interaction of Smo with cholesterol (14). In our studies, pretreatment with cholesterol overcame the capacity of vismodegib to inhibit Hh signaling in NIH 3T3 cells and MB cells, implying that cholesterol compromises the interaction between vismodegib and Smo. These data suggest an indirect competition between cholesterol and vismodegib, possibly through allosteric effects, in binding to Smo.

Treatment with Smo antagonists results in dramatic regression of tumor burden and reduction of symptoms, but there is a rapid emergence of drug-resistance (50). The resistance often arises as a consequence of mutations in the transmembrane domain of Smo that prevent binding of antagonists. Therefore, cholesterol inhibitors could not only synergize with vismodegib in treating MB, but also potentially be effective in treating some drug-resistant Hh-MB.

Supplementary Material

Refer to Web version on PubMed Central for supplementary material.

Acknowledgments

Authors would like to thank Dr. G. E. Herman and Dr. D. Cunningham (The Ohio State University, Columbus, OH) for providing *Nsdhl*$^{fl/fl}$ mice, Dr. T. Yen and Dr. E. Golemis for thoughtful comments, A. Efimov, E. Nicolas, F. Jin and J. Oesterling for technical assistance.

Funding: NCI (CA178380, CA185504), ACS RSG (RSG1605301NEC), PA CURE Health Research Fund, Bucks County Chapter, National Natural Science Foundation of China (81572724, 81573449). This research was supported by the subsidy of the Russian Government to support the Program of competitive growth of Kazan Federal University to Renata E. Gordon.

References

1. Dietschy JM, Turley SD. Cholesterol metabolism in the brain. Current opinion in lipidology. 2001; 12:105–112. [PubMed: 11264981]
2. Goldstein JL, Brown MS. Regulation of the mevalonate pathway. Nature. 1990; 343:425–430. [PubMed: 1967820]
3. Liu XY, et al. The gene mutated in bare patches and striated mice encodes a novel 3beta-hydroxysteroid dehydrogenase. Nat Genet. 1999; 22:182–187. [PubMed: 10369263]
4. Cunningham D, et al. Analysis of hedgehog signaling in cerebellar granule cell precursors in a conditional Nsdhl allele demonstrates an essential role for cholesterol in postnatal CNS development. Human molecular genetics. 2015; 24:2808–2825. [PubMed: 25652406]

5. Avigan J, Steinberg D, Vroman HE, Thompson MJ, Mosettig E. Studies of cholesterol biosynthesis. I. The identification of desmosterol in serum and tissues of animals and man treated with MER-29. The Journal of biological chemistry. 1960; 235:3123–3126. [PubMed: 13685286]
6. Fuse N, et al. Sonic hedgehog protein signals not as a hydrolytic enzyme but as an apparent ligand for patched. Proceedings of the National Academy of Sciences of the United States of America. 1999; 96:10992–10999. [PubMed: 10500113]
7. Kalderon D. Transducing the hedgehog signal. Cell. 2000; 103:371–374. [PubMed: 11081624]
8. Corcoran RB, Scott MP. Oxysterols stimulate Sonic hedgehog signal transduction and proliferation of medulloblastoma cells. Proceedings of the National Academy of Sciences of the United States of America. 2006; 103:8408–8413. [PubMed: 16707575]
9. Nachtergaele S, et al. Oxysterols are allosteric activators of the oncoprotein Smoothened. Nature chemical biology. 2012; 8:211–220. [PubMed: 22231273]
10. Nedelcu D, Liu J, Xu Y, Jao C, Salic A. Oxysterol binding to the extracellular domain of Smoothened in Hedgehog signaling. Nature chemical biology. 2013; 9:557–564. [PubMed: 23831757]
11. Myers BR, et al. Hedgehog pathway modulation by multiple lipid binding sites on the smoothened effector of signal response. Dev Cell. 2013; 26:346–357. [PubMed: 23954590]
12. Huang P, et al. Cellular Cholesterol Directly Activates Smoothened in Hedgehog Signaling. Cell. 2016; 166:1176–1187 e1114. [PubMed: 27545348]
13. Luchetti G, et al. Cholesterol activates the G-protein coupled receptor Smoothened to promote Hedgehog signaling. Elife. 2016; 5
14. Byrne EF, et al. Structural basis of Smoothened regulation by its extracellular domains. Nature. 2016; 535:517–522. [PubMed: 27437577]
15. Bar EE, Chaudhry A, Farah MH, Eberhart CG. Hedgehog signaling promotes medulloblastoma survival via Bc/II. Am J Pathol. 2007; 170:347–355. [PubMed: 17200206]
16. Dimitroulakos J, et al. Differential sensitivity of various pediatric cancers and squamous cell carcinomas to lovastatin-induced apoptosis: therapeutic implications. Clin Cancer Res. 2001; 7:158–167. [PubMed: 11205904]
17. Wang W, Macaulay RJ. Mevalonate prevents lovastatin-induced apoptosis in medulloblastoma cell lines. Can J Neurol Sci. 1999; 26:305–310. [PubMed: 10563217]
18. Takwi AA, et al. A statin-regulated microRNA represses human c-Myc expression and function. EMBO Mol Med. 2012; 4:896–909. [PubMed: 22887866]
19. Sasai K, et al. Shh pathway activity is down-regulated in cultured medulloblastoma cells: implications for preclinical studies. Cancer research. 2006; 66:4215–4222. [PubMed: 16618744]
20. Meyers-Needham M, et al. Off-target function of the Sonic hedgehog inhibitor cyclopamine in mediating apoptosis via nitric oxide-dependent neutral sphingomyelinase 2/ceramide induction. Mol Cancer Ther. 2012; 11:1092–1102. [PubMed: 22452947]
21. Tomayko MM, Reynolds CP. Determination of subcutaneous tumor size in athymic (nude) mice. Cancer chemotherapy and pharmacology. 1989; 24:148–154. [PubMed: 2544306]
22. Yang ZJ, et al. Medulloblastoma can be initiated by deletion of Patched in lineage-restricted progenitors or stem cells. Cancer Cell. 2008; 14:135–145. [PubMed: 18691548]
23. Hanzelmann S, Castelo R, Guinney J. GSVA: gene set variation analysis for microarray and RNA-seq data. BMC Bioinformatics. 2013; 14:7. [PubMed: 23323831]
24. Leardi R. Experimental design in chemistry: A tutorial. Anal Chim Acta. 2009; 652:161–172. [PubMed: 19786177]
25. Thompson MC, et al. Genomics identifies medulloblastoma subgroups that are enriched for specific genetic alterations. Journal of clinical oncology: official journal of the American Society of Clinical Oncology. 2006; 24:1924–1931. [PubMed: 16567768]
26. Northcott PA, et al. Medulloblastoma comprises four distinct molecular variants. Journal of clinical oncology: official journal of the American Society of Clinical Oncology. 2011; 29:1408–1414. [PubMed: 20823417]

27. Akino T, et al. Netrin-1 promotes medulloblastoma cell invasiveness and angiogenesis, and demonstrates elevated expression in tumor tissue and urine of patients with pediatric medulloblastoma. Cancer research. 2014; 74:3716–3726. [PubMed: 24812271]
28. Goodrich LV, Milenkovic L, Higgins KM, Scott MP. Altered neural cell fates and medulloblastoma in mouse patched mutants. Science. 1997; 277:1109–1113. [PubMed: 9262482]
29. Wetmore C, Eberhart DE, Curran T. Loss of p53 but not ARF accelerates medulloblastoma in mice heterozygous for patched. Cancer research. 2001; 61:513–516. [PubMed: 11212243]
30. van der Wulp MY, Verkade HJ, Groen AK. Regulation of cholesterol homeostasis. Molecular and cellular endocrinology. 2013; 368:1–16. [PubMed: 22721653]
31. Venkateswaran A, et al. Control of cellular cholesterol efflux by the nuclear oxysterol receptor LXR alpha. Proceedings of the National Academy of Sciences of the United States of America. 2000; 97:12097–12102. [PubMed: 11035776]
32. Goldstein JL, DeBose-Boyd RA, Brown MS. Protein sensors for membrane sterols. Cell. 2006; 124:35–46. [PubMed: 16413480]
33. Mao X, Fujiwara Y, Chapdelaine A, Yang H, Orkin SH. Activation of EGFP expression by Cre-mediated excision in a new ROSA26 reporter mouse strain. Blood. 2001; 97:324–326. [PubMed: 11133778]
34. Yokota N, et al. Predominant expression of human zic in cerebellar granule cell lineage and medulloblastoma. Cancer research. 1996; 56:377–383. [PubMed: 8542595]
35. Ganat YM, et al. Early postnatal astroglial cells produce multilineage precursors and neural stem cells in vivo. J Neurosci. 2006; 26:8609–8621. [PubMed: 16914687]
36. Jeong J, Mao J, Tenzen T, Kottmann AH, McMahon AP. Hedgehog signaling in the neural crest cells regulates the patterning and growth of facial primordia. Genes & development. 2004; 18:937–951. [PubMed: 15107405]
37. Gajjar A, et al. Phase I study of vismodegib in children with recurrent or refractory medulloblastoma: a pediatric brain tumor consortium study. Clinical cancer research: an official journal of the American Association for Cancer Research. 2013; 19:6305–6312. [PubMed: 24077351]
38. Robinson GW, et al. Vismodegib Exerts Targeted Efficacy Against Recurrent Sonic Hedgehog-Subgroup Medulloblastoma: Results From Phase II Pediatric Brain Tumor Consortium Studies PBTC-025B and PBTC-032. Journal of clinical oncology: official journal of the American Society of Clinical Oncology. 2015; 33:2646–2654. [PubMed: 26169613]
39. Xie J, et al. Activating Smoothened mutations in sporadic basal-cell carcinoma. Nature. 1998; 391:90–92. [PubMed: 9422511]
40. Kool M, et al. Genome sequencing of SHH medulloblastoma predicts genotype-related response to smoothened inhibition. Cancer Cell. 2014; 25:393–405. [PubMed: 24651015]
41. Schuller U, et al. Acquisition of granule neuron precursor identity is a critical determinant of progenitor cell competence to form Shh-induced medulloblastoma. Cancer Cell. 2008; 14:123–134. [PubMed: 18691547]
42. Robarge KD, et al. GDC-0449-a potent inhibitor of the hedgehog pathway. Bioorg Med Chem Lett. 2009; 19:5576–5581. [PubMed: 19716296]
43. Kimura H, Ng JM, Curran T. Transient inhibition of the Hedgehog pathway in young mice causes permanent defects in bone structure. Cancer Cell. 2008; 13:249–260. [PubMed: 18328428]
44. Kuzu OF, Noory MA, Robertson GP. The Role of Cholesterol in Cancer. Cancer research. 2016; 76:2063–2070. [PubMed: 27197250]
45. Villa GR, et al. An LXR-Cholesterol Axis Creates a Metabolic Co-Dependency for Brain Cancers. Cancer Cell. 2016; 30:683–693. [PubMed: 27746144]
46. Bidet M, et al. The hedgehog receptor patched is involved in cholesterol transport. PloS one. 2011; 6:e23834. [PubMed: 21931618]
47. Pei Y, et al. HDAC and PI3K Antagonists Cooperate to Inhibit Growth of MYC-Driven Medulloblastoma. Cancer Cell. 2016; 29:311–323. [PubMed: 26977882]
48. Eiland LS, Luttrell PK. Use of statins for dyslipidemia in the pediatric population. J Pediatr Pharmacol Ther. 2010; 15:160–172. [PubMed: 22477808]

49. Wiegman A, et al. Efficacy and safety of statin therapy in children with familial hypercholesterolemia: a randomized controlled trial. JAMA. 2004; 292:331–337. [PubMed: 15265847]

50. Rudin CM, et al. Treatment of medulloblastoma with hedgehog pathway inhibitor GDC-0449. The New England journal of medicine. 2009; 361:1173–1178. [PubMed: 19726761]

Translational Relevance

Medulloblasotma (MB) is the most common malignant brain tumor in children. Approximately 30% of human MB arise from aberrant activation of hedgehog (Hh) pathway. Vismodegib and sonidegib are two FDA-approved Hh pathway inhibitors, that have demonstrated efficacy in clinical trials of Hh pathway-associated MB (Hh-MB). Despite a dramatic response to these inhibitors in initial clinical trails, drug resistance and developmental toxicities, arise in humans as predicted by mouse models. Here we demonstrate that cholesterol is required for Hh pathway signal transduction in tumor cells. Statins, inhibitors of cholesterol biosynthesis, block hedgehog pathway activity in MB and synergize with vismodegib to inhibit tumor growth. Given the excellent safety profile, low cost and ready availability of cholesterol inhibitors, targeting cholesterol biosynthesis represents a promising strategy for treatment of Hh-MB and potentially other malignancies caused by Hh pathway activation.

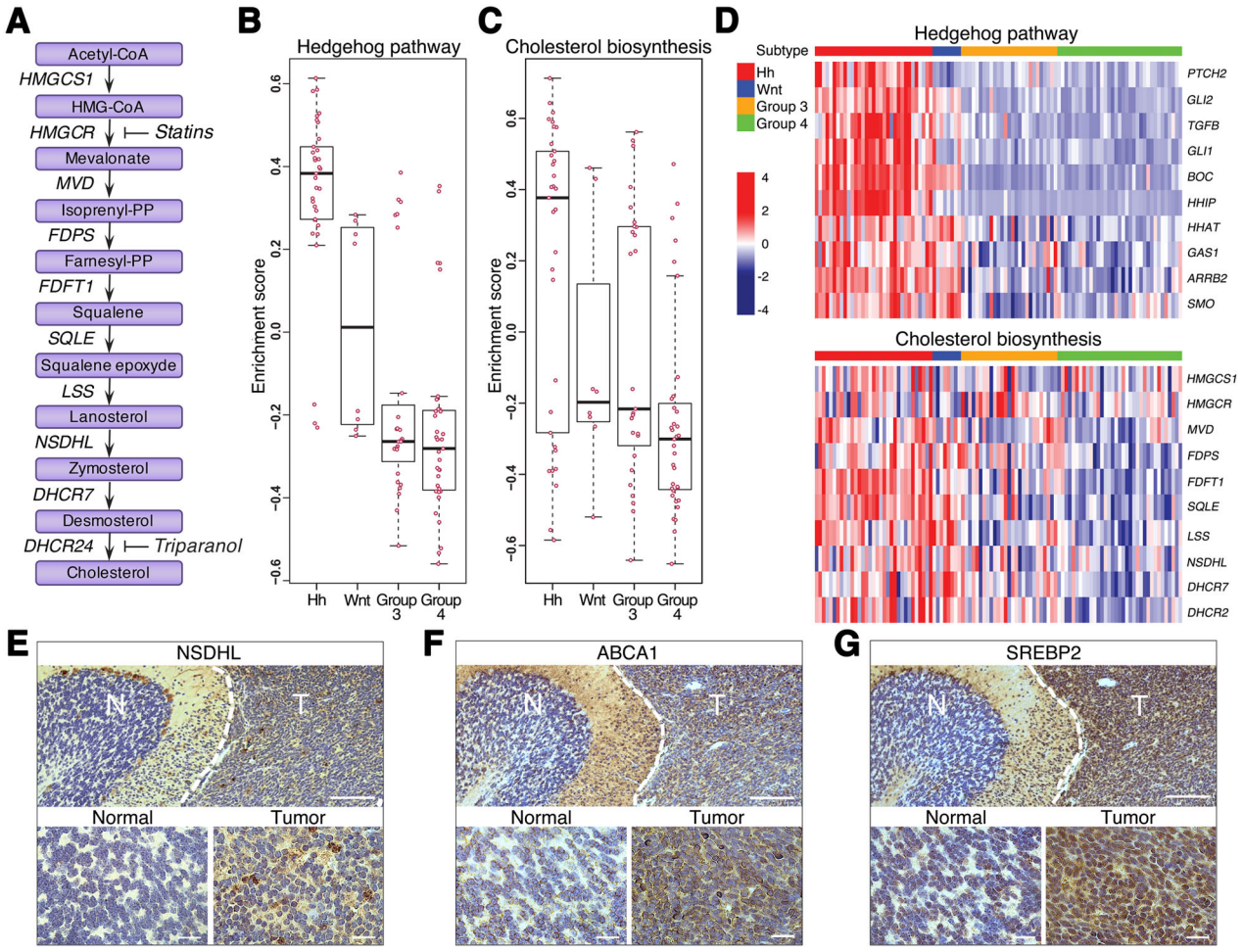

Fig. 1. Cholesterol biosynthesis is enhanced in Hh subtype of MB

(A) A schematic diagram of cholesterol biosynthesis pathway with genes encoding corresponding enzymes listed along arrows. Enzymes: HMGCS1 3-hydroxy-3-methylglutaryl-CoA synthase 1; HMGCR 3-hydroxy-3-methylglutaryl-CoA reductase; MVD mevalonate diphosphate decarboxylase; FDPS farnesyl diphosphate synthase; FDFT1 farnesyl-diphosphate farnesyltransferase 1; SQLE squalene epoxidase; LSS lanosterol synthase; NSDHL NAD(P) dependent steroid dehydrogenase-like; DHCR7 7-dehydrocholesterol reductase; DHCR24 24-dehydrocholesterol reductase.
Statins inhibit conversion of HMG-CoA to mevalonate through competitive inhibition of HMG-CoA reductase (HMGCR). Triparanol blocks the last step of cholesterol biosynthetic pathway through inhibition of 24-dehydrocholesterol reductase (DHCR24).
(B–C) Box plots showing the enrichment scores from Gene Set Variation Analysis. X and Y-axes illustrate enrichment statistics across 4 different subtypes of MB. Positive and negative scores indicate positive and negative enrichment respectively. Pink dots represent the enrichment score for each sample in that subtype. Black bar in the middle of the box indicates median.

(D) Heat maps showing expression of representative genes in the Hh and cholesterol synthesis pathways. Z-scores calculated for each gene are plotted on a red (higher expression) and blue (low expression) scale. Top color bar indicates the subtype. **(E–G)** Immunohistochemical analysis of NSDHL (E), ABCA1 (F) and SREBP2 (G) proteins in mouse *Ptch1*$^{+/-}$ MB. Normal adjacent tissue represents a cerebellar lobe with differentiated granule neurons used as a control. Scale bars 100 μm, insets 10 μm.

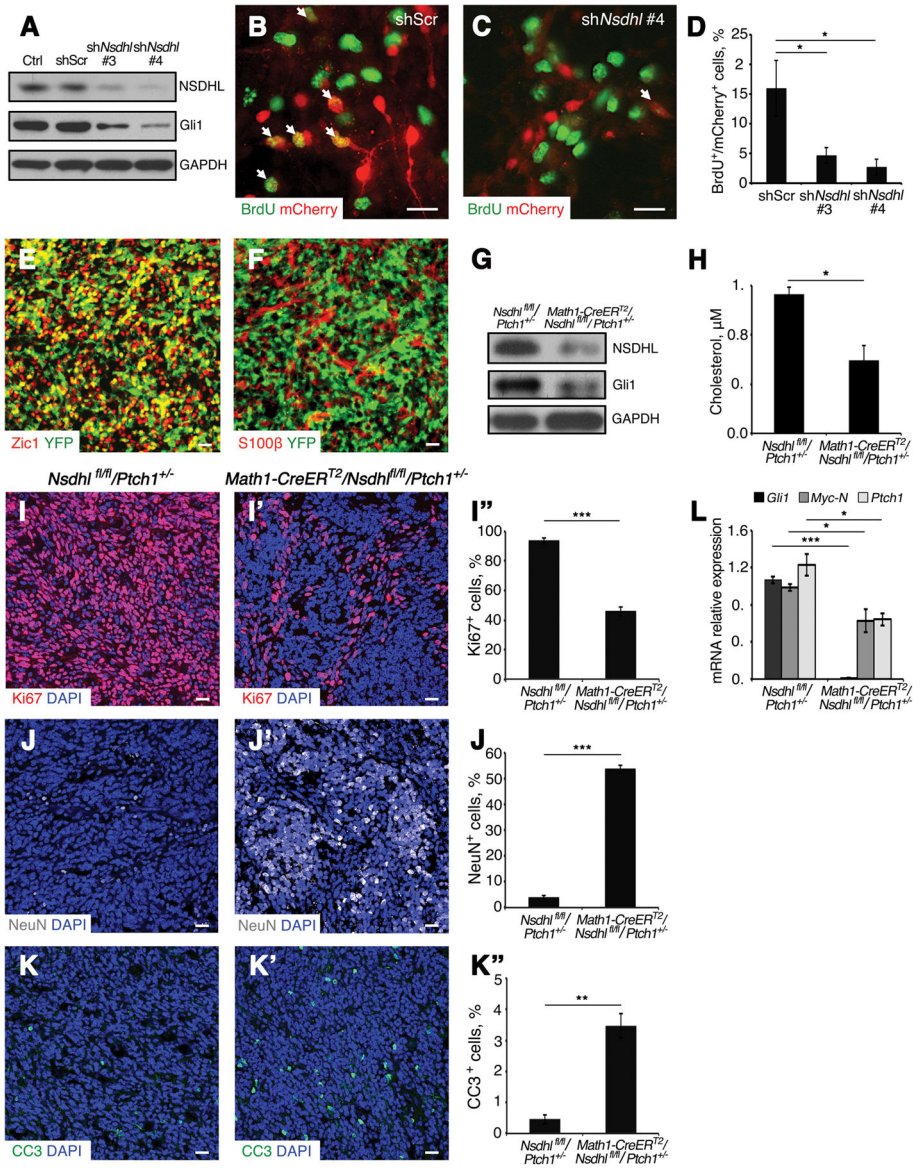

Fig. 2. Deficiency of NSDHL inhibits *Ptch1*$^{+/-}$ MB cell proliferation

(A) Western blot analysis of NSDHL and Gli1 proteins expression in *Ptch1*$^{+/-}$ MB cells following infection with lentivirus carrying *Nsdhl* shRNA (#3 and #4) or scrambled shRNA and uninfected control after 48 hours in culture. GAPDH was used as a loading control.

(B–C) Immunofluorescence analysis of BrdU among *Ptch1*$^{+/-}$ MB cells infected with scrambled control shRNA (mCherry^{+}, B) or *Nsdhl* shRNA #4 (mCherry^{+}, C) after 48 hours in culture.

(D) Percentage of BrdU^{+} cells in infected MB cells (mCherry^{+}) in Fig. 3B and 3C.

(E–F) Sagittal sections of MB tissue from *Math1-CreER*^{T2}*/R26R-eYFP/Ptch1*$^{+/-}$ mice were immunostained against Zic1 and YFP (E), S100β and YFP (F).

(G) Western blot analysis of NSDHL and Gli1 protein expression in MB tissue from *Math1-CreER*^{T2}*/Nsdhl* $^{fl/fl}$*/Ptch1*$^{+/-}$ and *Nsdhl*$^{fl/fl}$*/Ptch1*$^{+/-}$ mice after tamoxifen treatment. GAPDH was used as a loading control.

(H) Mass-spectrometry analysis of cholesterol content (μM) in MB tissue from *Math1-CreER^{T2}/Nsdhl $^{fl/fl}$/Ptch1$^{+/-}$* mice and *Nsdhl$^{fl/fl}$/Ptch1$^{+/-}$* mice after tamoxifen treatment.
(I–K″) Immunofluorescence analysis of Ki67 (I–I″), NeuN (J–J″) and CC3 (K–K″) in tumor tissue from *Nsdhl $^{fl/fl}$/Ptch1$^{+/-}$* mice (I, J, K), *Math1-CreER^{T2}/Nsdhl $^{fl/fl}$/Ptch1$^{+/-}$* mice (I′, J′, K′) after tamoxifen treatment, and percentage of Ki67, NeuN and CC3 positive cells in above sections respectively (I″, J″, K″). MB tissues were counterstained with DAPI.
(L) qPCR analysis of relative mRNA expression of Hh pathway genes (*Gli1, N-Myc, Ptch1*) in MB tissue from *Math1-CreER^{T2}/Nsdhl $^{fl/fl}$/Ptch1$^{+/-}$* mice and *Nsdhl $^{fl/fl}$/Ptch1$^{+/-}$* mice after tamoxifen treatment.
Scale bars 10 μm. Significance asterisk key: p value < 0.05 (*), p<0.01 (**), p<0.001 (***), p<0.0001 (****).

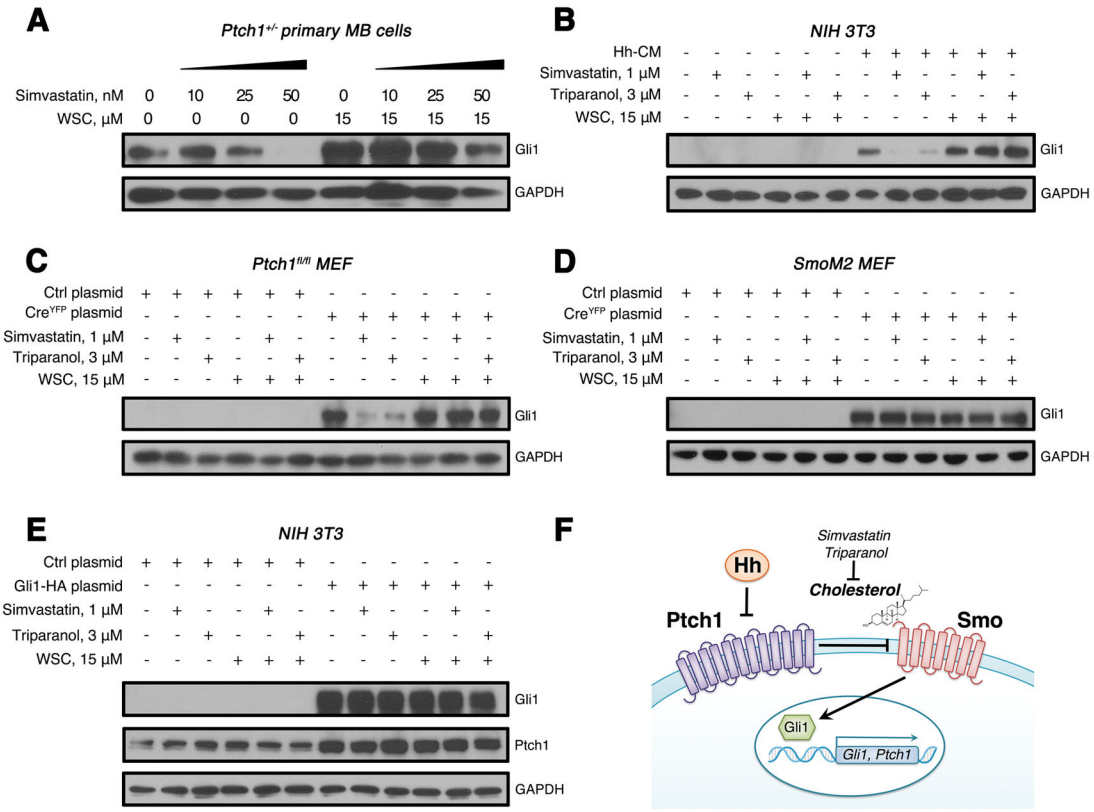

Fig. 3. Cholesterol is required for Smo activation in Hh signal transduction

(A) Western blot analysis of Gli1 protein expression in *Ptch1*$^{+/-}$ MB cells following treatment with simvastatin alone or in combination with WSC for 48 hours.

(B) Western blot analysis of Gli1 protein expression in NIH 3T3 cells following treatment with Hh-CM, simvastatin, triparanol or together with WSC for 48 hours.

(C–D) Western blot analysis of Gli1 protein expression in *Ptch1*$^{fl/fl}$ MEFs (C) or *SmoM2* MEFs (D) infected with a lentivirus carrying Cre recombinase or control empty vector following treatment with simvastatin, triparanol or WSC for 48 hours.

(E) Western blot analysis of Gli1 and Ptch1 proteins in NIH 3T3 cells infected with a lentivirus carrying a Gli1-HA construct or an empty vector following treatment with simvastatin, triparanol or WSC for 48 hours. GAPDH was used as a loading control.

(F) A schematic diagram of Hh signaling pathway. In the absence of Hh ligand, its receptor Ptch1 tethers Smo, preventing the downstream activation of Hh pathway. After interaction with Hh, Ptch1 releases Smo, causing activation of Gli1/2 transcription factor and leading to transcription of Hh pathway genes (*Gli1, Ptch1*, etc.). Cholesterol is required for Smo activation in Hh signal transduction.

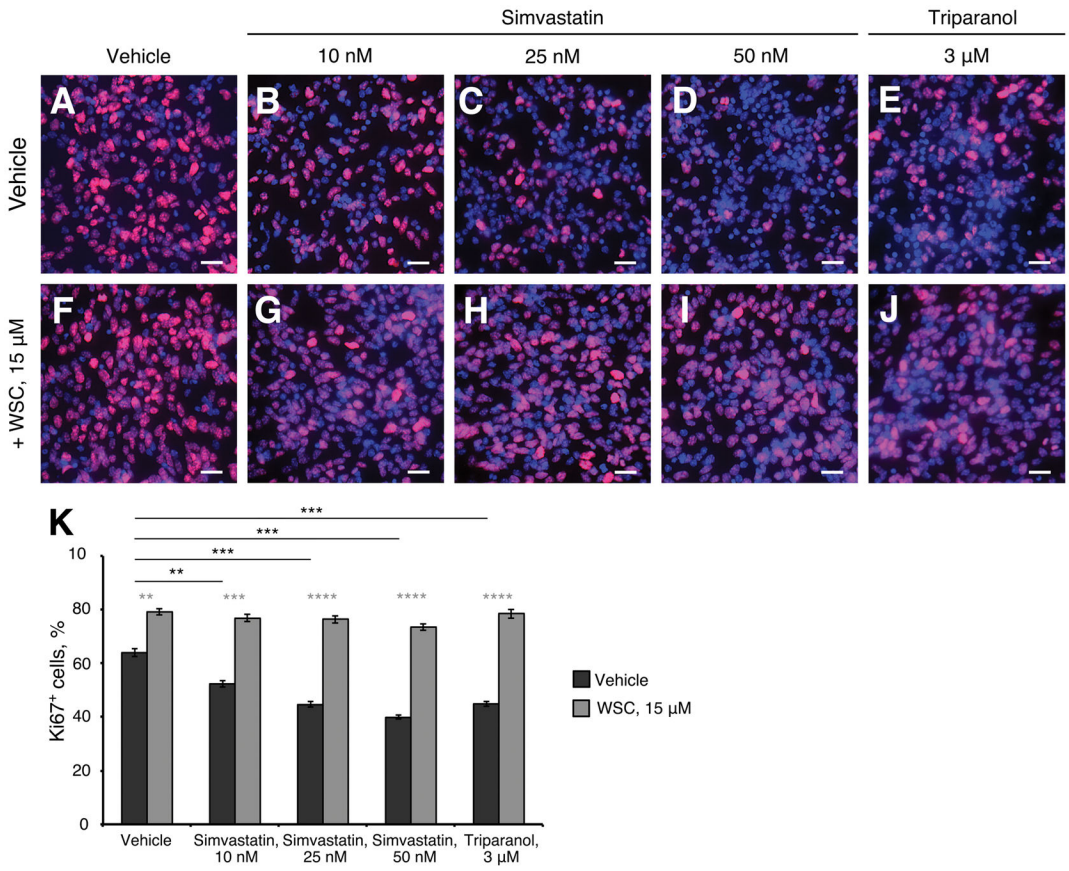

Fig. 4. Cholesterol biosynthesis inhibitors suppress proliferation of *Ptch1*$^{+/-}$ MB cells

(A–K) MB cells isolated from *Ptch1*$^{+/-}$ mouse were cultured in presence of vehicle **(A)** or simvastatin **(B–D)**, triparanol **(E)**, or together with WSC **(F–J)** for 48 hours, before cultured cells were immunostained against Ki67 (red) and counterstained with DAPI. Scale bars 10 μm.

(K) Percentage of Ki67 positive cells in cultured *Ptch1*$^{+/-}$ MB cells in presence of simvastatin, triparanol or with addition of WSC.

Significance asterisk key: p value < 0.05 (*), p<0.01 (**), p<0.001 (***), p<0.0001 (****).

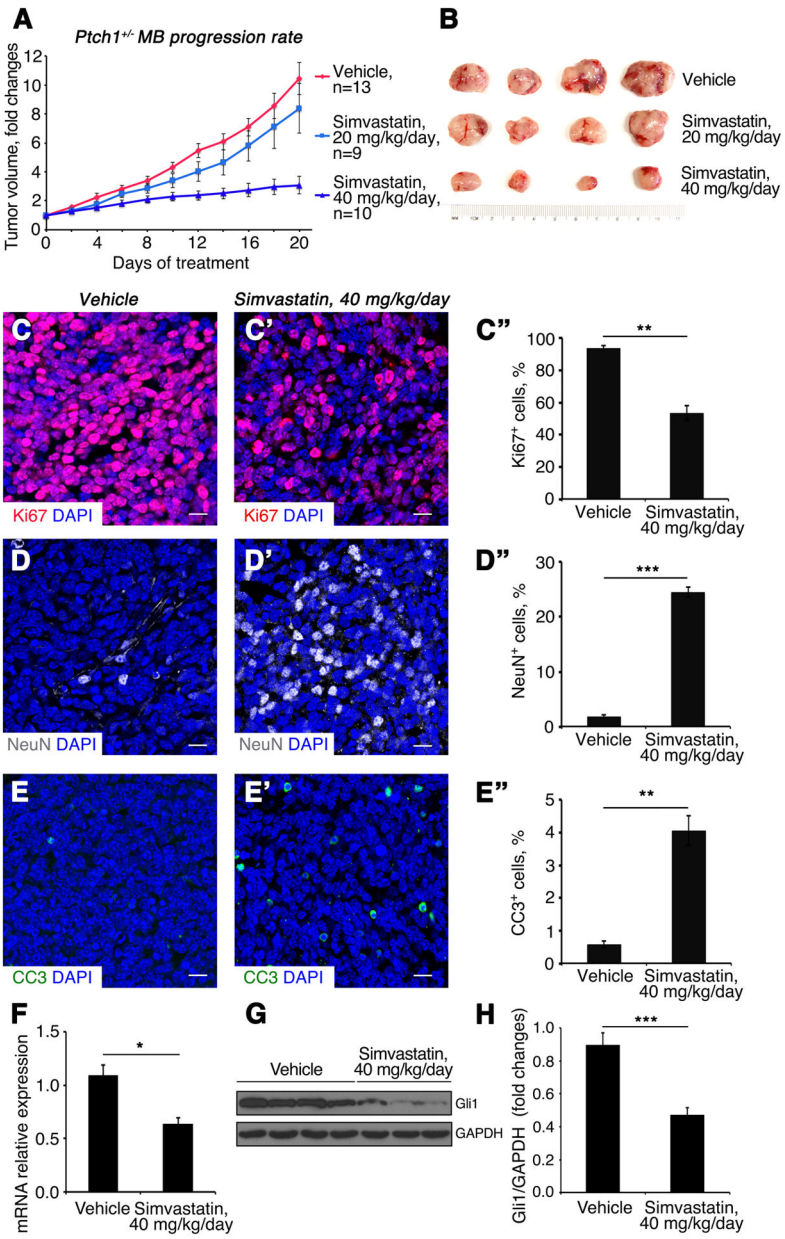

Fig. 5. Simvastatin inhibits growth of *Ptch1*$^{+/-}$ MB

(A) Growth rate of subcutaneous *Ptch1*$^{+/-}$ MB following treatment with simvastatin or vehicle control.

(B) Tumors size of subcutaneous *Ptch1*$^{+/-}$ MB following drug treatment.

(C–E″) Sections of subcutaneous *Ptch1*$^{+/-}$ MB after treatment with vehicle **(C, D, E)** or 40 mg/kg/day simvastatin **(C′, D′, E′)**, were immunostained for Ki67 (C–C″), NeuN (D–D″) or CC3 (E–E″). Percentage of Ki67^{+} cells (C″), NeuN^{+} cells (D″) and CC3^{+} cells (E″) in MB tissue after designated drug treatment. MB tissues were counterstained with DAPI. Scale bars 10 μm.

(F–H) mRNA (F) and protein (G) expression of Gli1 in *Ptch1*$^{+/-}$ MB tissues after drug treatment, were analyzed by qPCR and western blotting, respectively. (H) Quantification of Gli1 protein expression.

Significance asterisk key: p value < 0.05 (*), p<0.01 (**), p<0.001 (***), p<0.0001 (****).

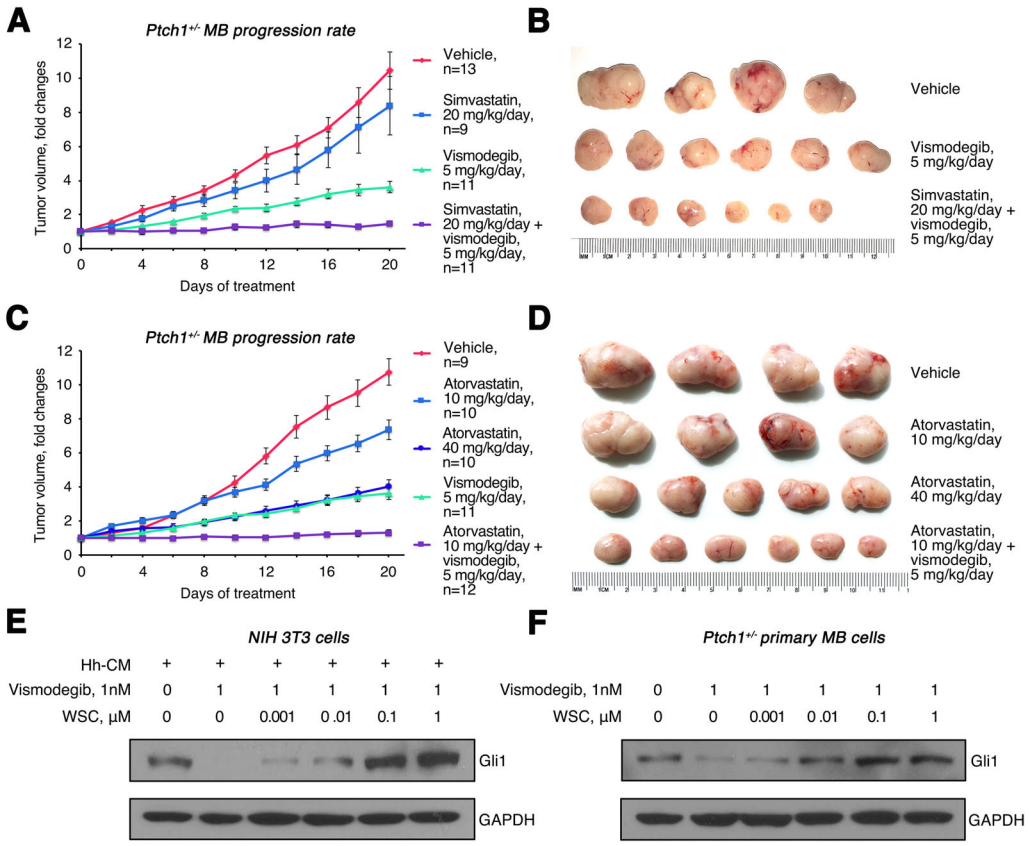

Fig. 6. Statins synergize with vismodegib in inhibiting *Ptch1*$^{+/-}$ MB growth

(A–B) Growth rate (A) and size (B) of subcutaneous *Ptch1*$^{+/-}$ MB treated with 20 mg/kg/day simvastatin, 5 mg/kg/day vismodegib or in combination. **(C–D)** Growth rate (C) and size (D) of subcutaneous *Ptch1*$^{+/-}$ MB treated with 10 mg/kg/day, 40 mg/kg/day atorvastatin, 5 mg/kg/day vismodegib or in combination. **(E)** Western blot analysis of Gli1 protein expression in NIH 3T3 cells treated with vismodegib for 48 hours following overnight treatment with WSC and Hh-CM. **(F)** Western blot analysis of Gli1 protein expression in *Ptch1*$^{+/-}$ MB cells treated with vismodegib for 48 hours after overnight treatment with WSC.